



Graphene oxide enhanced amine-functionalized titanium metal organic framework for visible-light-driven photocatalytic oxidation of gaseous pollutants



Xinru Li^{a,b}, Zaiyuan Le^{a,b}, Xiaolang Chen^b, Zhaoqing Li^b, Wenchao Wang^b, Xiaoyan Liu^b, Ao Wu^b, Pengcheng Xu^a, Dieqing Zhang^{b,*}

^a Department of Chemical and Biomolecular Engineering, University of California, Los Angeles, CA, 90095, United States

^b Key Laboratory of Resource Chemistry of Ministry of Education, Shanghai Key Laboratory of Rare Earth Functional Materials, Shanghai Normal University, Shanghai, 200234, China

ARTICLE INFO

Keywords:

Graphene oxide
NH₂-MIL-125(Ti)
Visible-light
Photocatalytic
Nitric oxide

ABSTRACT

Graphene oxide (GO) enhanced amine-functionalized titanium metal organic framework (NH₂-MIL-125(Ti)) was fabricated via a facile microwave solvothermal process by using GO, C₁₂H₂₈O₄Ti, and 2-aminoterephthalic acid as precursors. Under the microwave irradiation, the surface of GO could act as the microwave antenna for fast absorbing microwave energy with the formation of hot-spots on GO (hot-spots effect). These hot-spots allowed both the well-crystallization of NH₂-MIL-125(Ti) crystals with a highly dispersity on the surface of GO and the strong interaction between NH₂-MIL-125(Ti) and GO, supported by various characterization such as XRD, Raman, UV-vis and so on. Benefiting from the strong interaction and high electronic conductivity of GO, such GO/ NH₂-MIL-125(Ti) hybrid exhibited a greatly enhanced metal organic framework crystallinity, visible-light absorption, photocurrent intensity, electron carrier density and a lower photo-generated electron-hole recombination rate, compared to the pure NH₂-MIL-125(Ti). Therefore, the as-obtained hybrid system was proved highly efficient for photocatalytic oxidation of gaseous pollutants, such as nitric oxide (NO_x) and acetaldehyde with long durability, under visible light ($\lambda > 420$ nm) irradiation.

1. Introduction

Metal organic frameworks (MOF), as a new type of microporous materials built up from organic linkers and inorganic active centers, have attracted lots of attentions on the extensive applications in various fields, including adsorption [1,2], catalysis [3,4], H₂ [5] or CO₂ [6,7] storage, separation [8–10], and chemical sensors [11,12], due to the merits such as large surface areas, large pore volumes, diverse functionalization of pore, and functionalization of diversification. Among them, MIL-125 (Ti) exhibited special photo or catalytic properties, such as photochromic behavior [13], photocatalytic reduction of water to hydrogen gas [14–17], selective oxidation [18,19], and desulfurization [20]. Recently, more explorations on the application of MIL-125 (Ti) have been extended to photoelectrocatalytic detection of herbicide clethodim through an amino functionalization with the formation of NH₂-MIL-125 (Ti) owing to the inclusion of amine moieties and the extended absorption spectra into visible-light region [21].

Nevertheless, NH₂-MIL-125 (Ti), as a photocatalyst, still suffers from the fast recombination of photogenerated electrons and the cluster-

centers (Ti), resulting poor photocatalytic/photoelectrocatalytic performance for the further utilization in both environmental remediation and energy production based on the reduction of protons. Thus, it is highly required for searching an effective way to inhibit the electron-hole recombination while keeping the photo-response property of NH₂-MIL-125 (Ti) unchanged. It is lucky that the graphene oxide (GO) has been proved as the conductive carbon materials for effectively improving the semiconductor photocatalytic performance via accelerating the electron-transfer [22–25].

Meanwhile, GO, as an alternative of soft carbon material, also possesses the various characteristics of colloids, polymer films, as well as the amphoteric molecules, allowing it to contain rich functional groups, such as epoxy groups and hydroxyl groups. These groups on GO may serve as the nucleations for the fabrication of NH₂-MIL-125(Ti), ensuring a good dispersion of the as-obtained MOF crystals on the surface of GO. Considering that GO is also an excellent microwave absorbing materials owing to its high permittivity [26]. Even under 1 Hz irradiation, its dielectric constants still can be maintained about 689 [27]. Thus, it is reasonable that GO could serve as an antenna for

* Corresponding author.

E-mail address: dqzhang@shnu.edu.cn (D. Zhang).

absorbing microwave with the formation hot spots on the surface of GO, supplying a suitable and benign thermal condition for the growth of NH₂-MIL-125(Ti) with a high crystallinity [28,29].

In the present work, a microwave-induced fast route was proposed for the *in-situ* fabrication of NH₂-MIL-125(Ti) loaded on GO nanosheets substrates. By using such a route, mono-dispersed NH₂-MIL-125(Ti) with high crystallinity were closely bonded to the surface of GO. The aggregation of NH₂-MIL-125(Ti) was effectively prevented in the presence of GO matrix, allowing the MOF particles dispersed on GO layers. Such GO/NH₂-MIL-125(Ti) composites exhibited an obviously enhanced photocatalytic activity for treating the gaseous pollutants (NO_x and acetaldehyde) compared to the pure NH₂-MIL-125(Ti) owing to the greatly enhanced visible-light adsorption capability, photocurrent intensity, electron carrier density, strong heterojunctions, and low electron-hole recombination rates.

2. Experimental method

2.1. Materials and reagents

2-Aminoterephthalic acid (H₂ATA) were purchased from Sigma-Aldrich. Titanium isopropoxide (C₁₂H₂₈O₄Ti), dimethylformamide (DMF), and ethanol were purchased from Aladdin. These reagents were analytical grade and used without further purifications. Graphene oxide was prepared via a Hummers method [30].

2.2. The preparation of GO/NH₂-MIL-125 (Ti)

In a typical synthesis process, 1.0 g H₂ATA and 10.0 mg as-obtained GO were dispersed into a mixture solution containing 18.0 mL DMF and 3.0 mL methanol with strong stirring under ultrasound (Ultrasonication cleaner, 180 W, DS-3510DTH, Shanghai) at room temperature for 90 min. Then, 100 uL C₁₂H₂₈O₄Ti was added into the above mixture, while keeping stirring and ultrasonication for 10 min. The as-obtained mixture solution was further sealed in a 50 mL Teflon lined double-walled digestion vessel. After treating at 150 °C for 30 min using a microwave digestion system (Ethos TC, Milestone), the vessel was then cooled down to room temperature. The resulted suspension was centrifuged and washed with DMF and methanol, respectively. The as-obtained powders were further dried in air at 60 °C for achieving the final solid product (denoted as X-GO/NH₂-MIL-125 (Ti), X means the weight value in a unit of mg, X = 5, 10, 15, 20, and 25). For comparison, pure NH₂-MIL-125(Ti) was also synthesized by the same route in the absence of GO. Mechanical mixing samples were also prepared by mixing the 10 mg GO and the as-prepared NH₂-MIL-125(Ti) via grinding in air at room temperature. It was denoted as M10-GO/NH₂-MIL-125 (Ti).

2.3. Characterization

The morphology was observed via field emission scanning electron microscopy (FESEM, HITACHI S-4800) and transmission electronic micrograph (TEM, JEOL JEM-2100). UV-vis diffuse reflectance spectra (DRS) were obtained on a UV-vis spectra photometer (DRS, UV-2450). The Brunauer-Emmett-Teller (BET) approach was used to determine the surface area. X-ray photoelectron spectroscopy (XPS) was done on a PerkinElmer PHI 5000C ESCA system to analyze electronic states. All the binding energies were calibrated by using the contaminant carbon (C1s = 284.6 eV) as a reference. The Fourier transformation infra-red spectrum (FTIR) experiments were carried out on an AVATAR 370 FT-IR spectrometer. The photoluminescence spectroscopy (PLS) was collected on Varian Cary-Eclips 500 with an excitation light at 264 nm.

2.4. Photoelectrochemical (PEC) measurements

Photoelectrochemical measurements were performed in a three-

electrode, single-compartment quartz cell on an electrochemical station (CHI 660D). The GO and GO/NH₂-MIL-125 (Ti) electrodes (active area of 4 cm², coated on ITO glass) were utilized as the working electrodes. A platinum sheet (99.99%, 0.1 mm, 2 cm*2 cm) and saturated calomel electrode (SCE) were used as the counter electrode and reference electrode, respectively. A 300 W Xenon lamp ($\lambda > 420$ nm, with an ultraviolet filter), as the visible-light source, was positioned 10 cm away from the photoelectrochemical cell. Impedance measurements were performed under visible light illumination ($\lambda > 420$ nm) in a 0.5 mol/L Na₂SO₄ solution at open circuit voltage over a frequency range from 10⁵ to 10⁻¹ Hz with an AC voltage at 5 mV. The transient photocurrent was measured using a 20 s on-off cycle at a bias voltage of 0.5 V. The Mott-Schottky plots were obtained at a fixed frequency of 1 KHz to determine the flat-band potential and carrier density.

2.5. Activity test

The photocatalytic NO oxidation in gas phase was carried out at ambient temperature in a continuous flow reactor with volume of 4.5 L (10 × 30 × 15 cm). During visible light driven photocatalysis, 2*150 W tungsten halogen lamps (General Electric) located vertically above the reactor by cutting the lights with wavelength shorter than 420 nm using an ultraviolet filter [31]. In each test, an air gas flow containing 500 ppb NO was pumped through 0.10 g photocatalyst (coated onto a glass dish with a diameter of 15.0 cm) at the rate of 4.0 L/min. The desired humidity level of the NO flow was controlled at 70% (2100 ppmv) by passing the zero air streams through a humidification chamber. After reaching adsorption-desorption equilibrium on the photocatalyst, the lamp was turned on to start the photocatalysis reaction. The concentration of NO was continuously measured by using a chemiluminescence NO analyzer (Thermo Environmental Instruments Inc. Model 42i). The NO removal rate (%) was calculated based on the following equation: NO removal rate (%) = (C₀ - C)/C₀ × 100%, where C₀ and C refer to the NO concentration determined before and after reaction [32].

The photocatalytic oxidation of gaseous acetaldehyde was carried out in a self-designed stainless steel reactor with a quartz glass window at 25 °C. In a typical test, 50.0 mg photocatalyst was dispersed in 10 mL anhydrous ethanol in a watch glass under ultrasonication for 0.5 min, and dried at 80 °C for 15 min. The dried watch glass contained samples was transferred into the above reactor. Then, 5.0 uL acetaldehyde was rapidly injected the reactor with the formation of the simulated organic gas pollutant ([CH₃CHO] = 1.95 mg/L, after reaching the absorption-desorption equation). A 300 W Xenon lamp, with a 420 nm cutoff filter, was used as a visible-light source for driving the photo-oxidation reaction. The distance between the reactor and Xenon lamp is 15 cm. Each photocatalytic oxidation reaction was performed for 60 min, and the remained gas was sampled and analyzed using a gas chromatograph (Shimadzu, GC- 17 A) for determining the final concentration of acetaldehyde.

3. Results and discussion

The morphologies of GO, NH₂-MIL-125(Ti) and GO/NH₂-MIL-125(Ti) nanocomposites were analyzed by scanning electron microscope (SEM). As shown in Fig. 1a, the GO samples possessed a regular fold structure. The NH₂-MIL-125(Ti) was composed of aggregated flat spherical grains, with an average size of about 200 nm, as shown in Fig. 1b. Such aggregation could be well avoided by introducing GO. From Fig. 1c, highly dispersed grains were observed on the surface of GO. Moreover, the size of the NH₂-MIL-125(Ti) loaded on GO was lower than that of pure NH₂-MIL-125(Ti) sample.

The transmission electron microscopy (TEM) images of GO (Fig. 2a) support the assertion that the as-prepared GO exhibited a regular fold structure with a few layers thickness, suggested by the inset of Fig. 2a. Such appearance of fold structure is mainly due to the oxidation

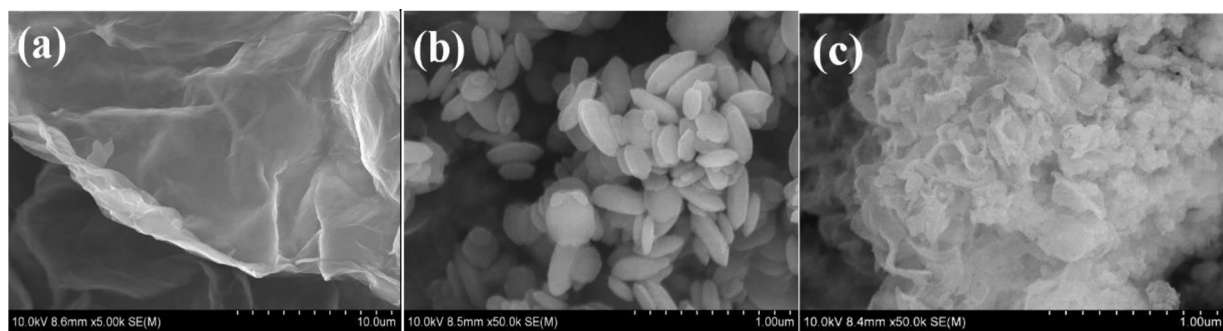


Fig. 1. FESEM image of (a) GO, (b) NH₂-MIL-125(Ti) and (c) 10-GO/NH₂-MIL-125(Ti).

process, which was introduced to the sp² hybrid carbon atoms in the sp³ hybridization of carbon atoms [30]. Two-dimensional plane of GO layer structure could be distorted by some carbon atoms connected with –OH groups, with the formation of fold of lamella. Flat spherical NH₂-MIL-125(Ti) crystals were obtained via the microwave thermal process, as shown in Fig. 2b, however, they still suffered a serious aggregation. It was interesting that these metal organic framework (MOF) crystals could be highly dispersed on the surface of GO (highlighted by white arrows) as shown in Fig. 2c. Compare to that of NH₂-MIL-125(Ti), the 10-GO/NH₂-MIL-125(Ti) sample possessed a smaller grain size of NH₂-MIL-125(Ti), probably because of the grain refinement in the microwave reaction process. This could be attributed to the microwave solvothermal process that the GO nanosheets could serve as an antenna for absorbing microwave with the formation of hot spots on the surface of GO (“hot-spots effect”), supplying a suitable and benign thermal condition for the growth of NH₂-MIL-125(Ti). The high resolution images of 10-GO/NH₂-MIL-125(Ti), as shown in Fig. 2d, explicitly differentiated the GO skeleton from the NH₂-MIL-125(Ti) crystals. This also clearly indicated that strong interactions (heterojunctions) existed on the interface between GO and NH₂-MIL-125(Ti), owing to the hot-spots effect. Such heterojunctions would be favorable for enhancing the photocatalytic performance of NH₂-MIL-125(Ti).

For illustrating the crystal structure and morphology of the as-obtained pure and GO grafted NH₂-MIL-125(Ti) samples, X-ray diffraction

(XRD) was recorded as shown in Fig. 3a. Both of the two samples possessed the typical diffraction peaks of NH₂-MIL-125(Ti) [13,33], suggesting the formation of perfect NH₂-MIL-125(Ti) crystals on GO under the microwave solvothermal process. Nevertheless, it should be pointed out that the intensity of the main diffraction peak of 10-GO/NH₂-MIL-125(Ti) was much higher than that of the pure NH₂-MIL-125(Ti). This illustrated that greatly improved crystallinity of NH₂-MIL-125(Ti) could be produced in the presence of GO under microwave irradiation, probably because of the “hot-spots effect” of GO in microwave solvothermal process, allowing a better crystallization of NH₂-MIL-125(Ti). Moreover, it was also observed from the enlarged XRD pattern (the inset of Fig. 3) that the diffraction peaks of 10-GO/NH₂-MIL-125(Ti) shifted to a lower angle compared to that of pure NH₂-MIL-125(Ti). Thus, it is reasonable that strong interactions were formed between GO and NH₂-MIL-125(Ti) in the GO/NH₂-MIL-125(Ti) composites. The nitrogen adsorption-desorption isotherms were also obtained at 77 K for investigating the textural properties of the samples as shown in Fig. 3b. A typical type I adsorption isotherm was observed for the sample of pure NH₂-MIL-125(Ti) with a Langmuir surface area of ca. 871 m²/g, indicating zeolite/zeolite-like crystalline solids were obtained in the present work according to the IUPAC classification [34]. Such MOF microstructure could be well maintained even after introducing GO under microwave-irradiation because 10-GO/NH₂-MIL-125(Ti) still possesses a type I adsorption isotherm shape, though

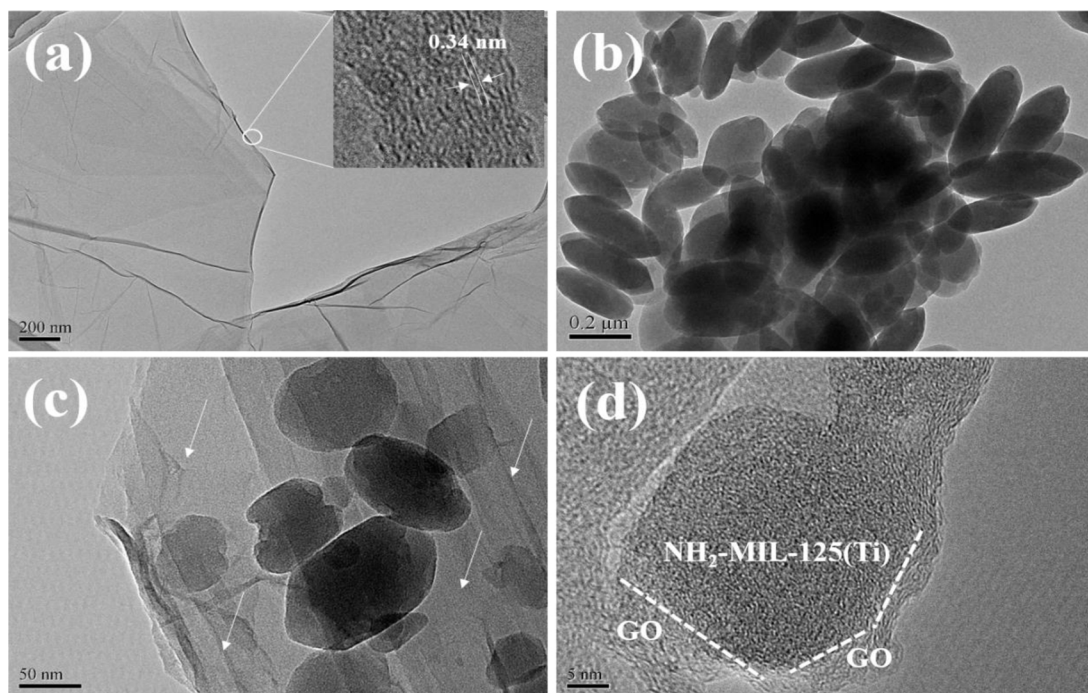


Fig. 2. TEM image and HRTEM image (inset) of GO (a), NH₂-MIL-125(Ti) (b), and 10-GO/NH₂-MIL-125(Ti) (c, d).

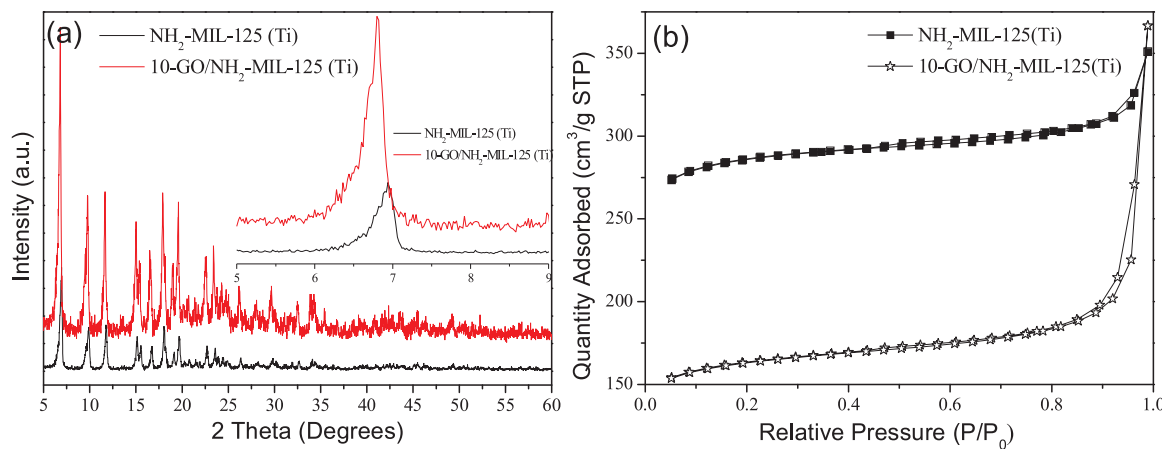


Fig. 3. The XRD patterns (a) and the N_2 adsorption-desorption isotherms (b) of $\text{NH}_2\text{-MIL-125(Ti)}$ and 10-GO/ $\text{NH}_2\text{-MIL-125(Ti)}$.

exhibiting a lower Langmuir surface area $502 \text{ m}^2/\text{g}$ was produced. Such high surface area could play an important role in both enhancing the light absorption capability and supplying an enough high active sites for driving the photocatalytic reactions [35].

For further detecting the composition of the as-obtained materials, the Fourier transform infrared spectroscopy (FTIR) spectra of GO, $\text{NH}_2\text{-MIL-125(Ti)}$ and 10-GO/ $\text{NH}_2\text{-MIL-125(Ti)}$ in the region of $450\text{--}4000 \text{ cm}^{-1}$ measured at room temperature were shown in Fig. 4a. The spectrum of the as-obtained GO (black trace) presented the characteristic bands of O–H stretching vibrations (3420 cm^{-1}), C=O stretching vibration (1740 cm^{-1}), C=C from un-oxidized sp^2 CC bonds (1620 cm^{-1}), C–OH vibration (1400 cm^{-1}) and C–O–C vibrations (1080 cm^{-1}) [22,36]. Such vibration absorption peaks indicated that regular oxidized graphene phase was achieved. The FTIR spectra of $\text{NH}_2\text{-MIL-125(Ti)}$ exhibited the characteristics of the stretching vibrations of the hydroxyl at 3450 cm^{-1} , the amino at 3350 cm^{-1} , the carboxylate in $1380\text{--}1600 \text{ cm}^{-1}$, and (O–Ti–O) vibrations in $400\text{--}800 \text{ cm}^{-1}$ [37].

The carboxylates stretching vibrations can be defined doublet bands (at 1530 and 1430 cm^{-1}), assigned to the COO⁻ antisymmetric and symmetric stretching vibrations complexed with surface Ti centers [22,38]. Upon being combined with GO, the FTIR spectrum of 10-GO/ $\text{NH}_2\text{-MIL-125(Ti)}$ exhibited a strong doublet bands of the COO⁻ anti-symmetric and symmetric stretching vibrations, indicating that $\text{NH}_2\text{-MIL-125(Ti)}$ crystals were closely bonded with GO through carboxylates. As known, Raman spectroscopy has been proved effective for the

investigation and detailed characterization of graphitic materials for achieving various important information, including crystallite size, clustering of the sp^2 phase, the presence of $\text{sp}^2\text{-sp}^3$ hybridization, the introduction of chemical impurities and so on [39]. Thus, it was utilized to analyze the similarities and differences between GO and 10-GO/ $\text{NH}_2\text{-MIL-125 (Ti)}$ composites. As shown Fig. 4b, all of the samples exhibited the D bands at ca. 1310 cm^{-1} (disorder-induced vibrational mode) and the G bands at ca. 1600 cm^{-1} (the E2g vibration mode of the sp^2 -bonded graphitic carbons). It was noted that the intensity ratio of G band to D band (the I_G/I_D ratio, indicative of the degree of structural defects and a quantitative measurement of edge plane exposure) [39,40] was decreased from 1.01 to 0.84 upon growing $\text{NH}_2\text{-MIL-125 (Ti)}$ crystals on the surface of GO under microwave solvothermal process. This could indicate that the GO was partly reduced into graphene by $\text{NH}_2\text{-MIL-125 (Ti)}$ in the microwave solvothermal conditions. It should be pointed out that the mechanical mixing sample of M10-GO/ $\text{NH}_2\text{-MIL-125 (Ti)}$ exhibited a higher I_G/I_D ratio (0.93), compared to 10-GO/ $\text{NH}_2\text{-MIL-125 (Ti)}$. Such difference of I_G/I_D ratio could be attributed to the interactions strength between GO and $\text{NH}_2\text{-MIL-125 (Ti)}$. These results suggested that a strong interaction was produced in microwave solvothermal process between GO and $\text{NH}_2\text{-MIL-125 (Ti)}$, with the formation of heterojunctions probably facilitating the electron transfer from $\text{NH}_2\text{-MIL-125 (Ti)}$ to GO.

The UV-vis diffuse reflectance spectra (DRS) is a strong tool for evaluating the electronic state and photo-absorption capability of the photoactive materials [35]. Thus, we further used DRS to investigate

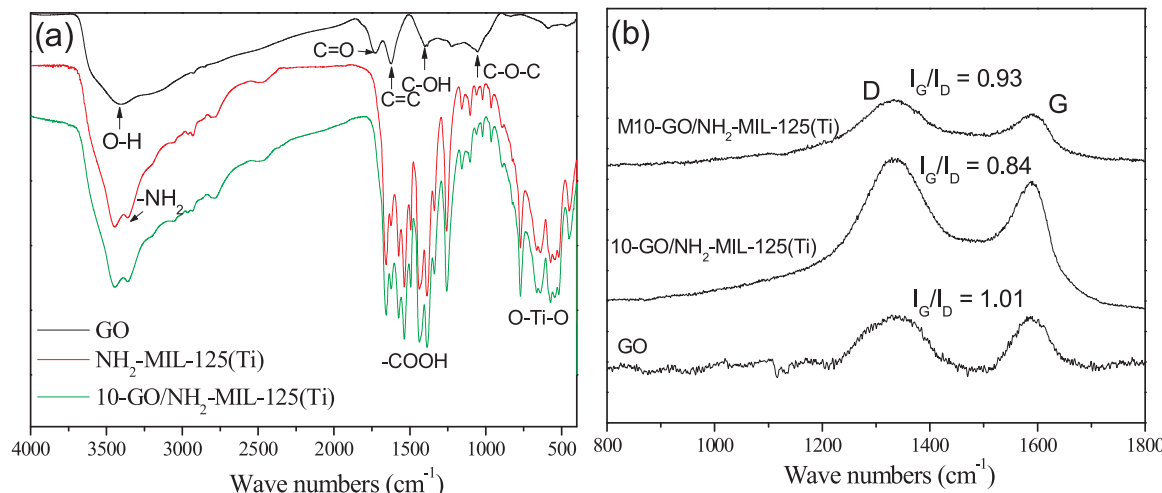


Fig. 4. (a) FTIR spectra of GO, $\text{NH}_2\text{-MIL-125(Ti)}$ and 10-GO/ $\text{NH}_2\text{-MIL-125(Ti)}$ and (b) Raman spectra of GO, 10-GO/ $\text{NH}_2\text{-MIL-125 (Ti)}$, and M10-GO/ $\text{NH}_2\text{-MIL-125 (Ti)}$.

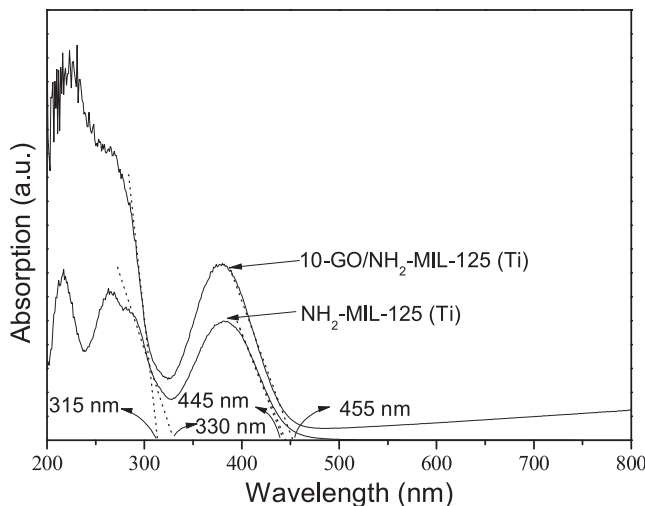


Fig. 5. UV-vis DRS spectra of NH₂-MIL-125(Ti) and 10-GO/NH₂-MIL-125(Ti).

the promotion effect of GO on the NH₂-MIL-125(Ti) crystals. As shown in Fig. 5, the as-formed NH₂-MIL-125(Ti) has two significant absorption peaks below 500 nm. The absorption band edges at about 330 nm (band gap energy of 3.76 eV) and 445 nm (band gap energy of 2.79 eV) were corresponding to the absorption of Ti–O oxo-clusters and the ligand-based absorption, respectively [41]. Upon being grafting on the surface of GO via a microwave solvothermal process, the absorption intensity of 10-GO/NH₂-MIL-125(Ti) in the range of 200–500 nm was greatly increased, indicating the introduction of GO may alter the background absorption into broad light region and improve the utilization of solar energy [42,43]. It was also noted that the absorption edge of Ti–O oxo-clusters shifted from 330 nm to about 315 nm, and the absorption edge of ligands shifted from 445 nm to 455 nm. The former (blue shift) could be attributed to the interaction between the carboxylates on GO and the Ti centers in NH₂-MIL-125(Ti). The later (red shift) indicated that the strong interaction between GO and NH₂-MIL-125(Ti) could alter the optical property of the ligands, with an extended light absorption region. Thus, we concluded that less energy of light can drive the as-prepared materials for photocatalytic reaction.

For better clarifying the promotion effect of GO on the photo-electronic property of the as-obtained samples, both electrochemical impedances spectroscopy (EIS) and photo-current response were evaluated by coating these samples on ITO glass. As known, charge-transfer process of the electrode can be illustrated by the semicircle in the Nyquist plot at high frequency, and the diameter of the semicircle may reflect the charge-transfer resistance. As shown in Fig. 6a, GO possessed the smallest arch owing to its excellent conductivity [44]. NH₂-MIL-125(Ti) exhibited the largest arch, however, such arch value could be greatly decreased after introducing GO, implying that decoration with GO may significantly enhance the electron mobility by reducing the recombination of electron-hole pairs. As shown in Fig. 6b, the photo-current density of 10-GO/NH₂-MIL-125(Ti) about 13 times of that of NH₂-MIL-125(Ti) under visible light ($\lambda > 420$ nm) irradiation, probably owing to the increased of light trapping capability and effective reduction of electron-hole pairs recombination rate. From Fig. 6a and b, one can find that the mechanical mixing sample (M10-GO/NH₂-MIL-125(Ti)) exhibited lower conductivity and photo-current compared to 10-GO/NH₂-MIL-125(Ti). This further supported that the effective combination of GO and NH₂-MIL-125(Ti) may greatly promote the separation of electron-hole pairs through the heterojunctions.

It is known that the PL signals of photo-responsive materials results from the recombination of photo-induced charge carriers. Thus, PL was proved as an effective technology for evaluating the performance of the photo-generated charge carrier trapping, migration, and transfer [45]. Generally, the exhibited lower PL intensity under light irradiation may

suggest the lower recombination rate of photo-generated electron-hole pairs [46,47]. The pure NH₂-MIL-125(Ti) sample displays a PL peak at around 528 nm, as shown in Fig. 7a. Such peak was greatly weakened upon being combined with GO via the microwave solvothermal treatment, indicating that the formation of GO/ NH₂-MIL-125(Ti) hybrids could significantly prohibit the photo-generated charge carrier recombination. The interaction between GO and NH₂-MIL-125(Ti) can create a new way to extend the service life of electronic-hole via facilitating the electron transfer through GO. Electron cannot return from excited state to ground state, thus directly weakening the photoluminescence intensity of NH₂-MIL-125(Ti). We also noted that the mechanical mixing sample, M10-GO/NH₂-MIL-125(Ti), exhibited a much higher PL intensity than 10-GO/NH₂-MIL-125(Ti) prepared via the microwave process. This could be ascribed to the weak interaction between GO and NH₂-MIL-125(Ti) via grinding treatment. Electrons cannot be well transferred due to the such weak interaction. This phenomenon related to the weak interaction resulting PL intensity was also proved by our previous reports [45]. For better comparing the electron carrier density (N_D) order of the as-obtained samples, Mott-Schottky plots were performed under visible-light irradiation ($\lambda > 420$ nm) as shown in Fig. 7b. Based on the Mott-Schottky equation:

$$N_D = [2C^2/(e^* \epsilon^* \epsilon_0)]^*(E - E_{FB} - K^*T/e)$$

where C is the space charge capacitance in the semiconductor, N_D is the electron carrier density, e is the elemental charge value, ϵ_0 is the permittivity of a vacuum, ϵ is the relative permittivity of the semiconductor, E is the applied potential, E_{FB} is the flat band potential, T is temperature, and k is the Boltzmann constant, it is reasonable that the N_D value of various samples was inversely proportional versus the slope of the tangent (dot lines in Fig. 7b) of Mott-Schottky plots [48,49]. The slopes of NH₂-MIL-125(Ti), M10-GO/NH₂-MIL-125(Ti), and 10-GO/NH₂-MIL-125(Ti) are 6.6656×10^7 , 6.2622×10^7 , and 5.5266×10^7 , respectively. Based on the above results, the ratio of N_D for various samples in the same order was calculated to be about 1: 1.064: 1.206. Such results proved that the strong interaction between GO and NH₂-MIL-125(Ti) could greatly enhance the electron carrier density, thus, 10-GO/NH₂-MIL-125(Ti) could serve as an excellent photocatalyst for driving catalytic process owing to its high electron transfer capability.

For evaluating the photocatalytic activity of the NH₂-MIL-125(Ti) based photocatalysts, the photo-oxidation of NO in a flow reactor was performed under visible light irradiation. As shown in Fig. 8a, the pure NH₂-MIL-125(Ti) sample exhibited a ca. 30% NO removal rate after about 30 min. Such value could be well maintained for continuous treating NO, suggesting NH₂-MIL-125(Ti) is a durable photocatalyst for oxidation NO under light irradiation. Upon introducing GO for loading NH₂-MIL-125(Ti), the photocatalytic activity was greatly enhanced. The optimal GO-loaded amount was proved to be 10 mg, with the formation a highest NO removal rate of about 50% for continuous oxidizing NO. Nevertheless, further increasing the amount of GO resulted in the decrease of the activity. To the case of 30-GO/NH₂-MIL-125(Ti), it took about 1 h to obtain a stable NO removal rate (33%), much lower than that of the optimal sample. It was ascribed to the excess GO, which resulted in less active photo-generated carriers and decreased activity of photocatalytic NO oxidation. More importantly, only trace NO₂ was detected during photocatalytic oxidation of 70% RH NO containing water vapor. On contrary, large amount of NO₂ was detected during photocatalytic oxidation of dried NO, indicating the important function of H₂O for the deep oxidation of NO. We also traced the activity of the mechanical mixing sample (M10-GO/NH₂-MIL-125(Ti)) for better comparison. As shown in Fig. 8a, it was found that loading GO in the sample of M10-GO/NH₂-MIL-125(Ti) cannot effectively improve the activity of NH₂-MIL-125(Ti) via a mechanical mixing process. Compared to the pure NH₂-MIL-125(Ti) sample, just slight increase of activity was observed. This suggested that the strong interaction between

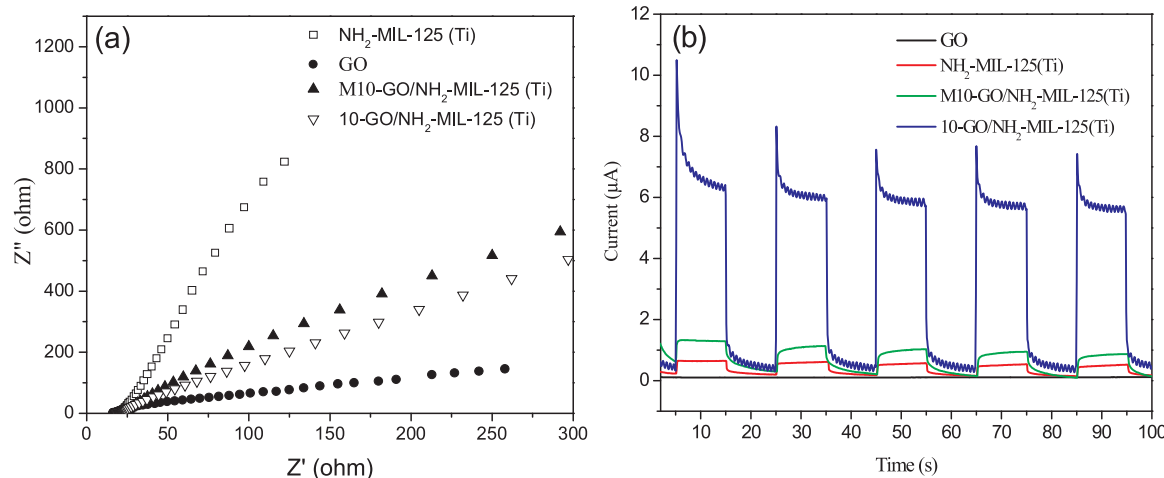


Fig. 6. (a) EIS Nynquist plots at open circuit potential, the x axis and y axis represent the real part of the impedance (Z') and the imaginary part of the impedance (Z''), respectively and (b) photo-current responses in the light on-off process (0.5 V vs. SCE) of various samples. All of the experiments performed using a 300 W Xe lamp irradiation ($\lambda > 420$ nm), with 3-electrode cell, immersed in a 0.5 M aqueous Na_2SO_4 electrolyte using Pt as counter electrode and saturated calomel electrode as reference electrode.

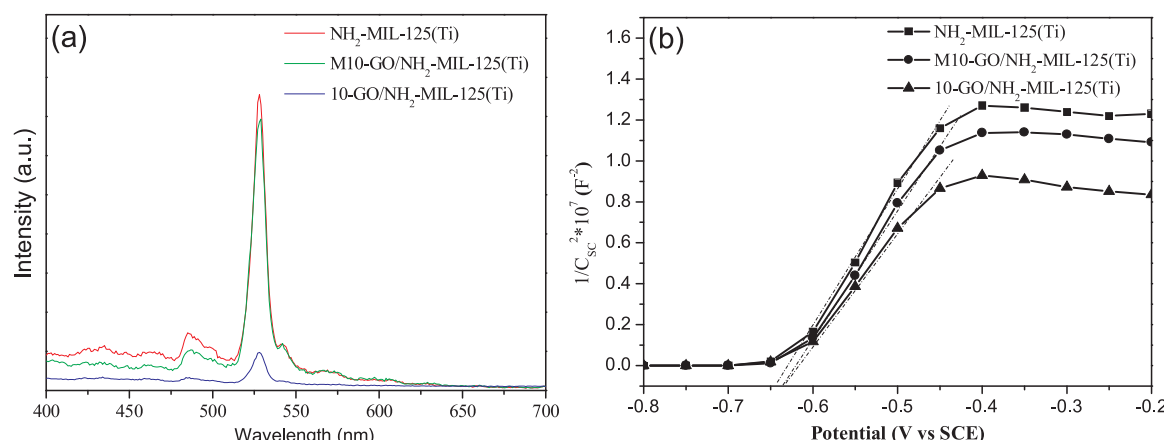


Fig. 7. Photoluminescence (PL) spectra (a) excited by 264 nm and Mott-Schottky plots obtained under visible-light irradiation ($\lambda = 420$ nm) of $\text{NH}_2\text{-MIL-125(Ti)}$, 10-GO/ $\text{NH}_2\text{-MIL-125(Ti)}$ and M10-GO/ $\text{NH}_2\text{-MIL-125(Ti)}$.

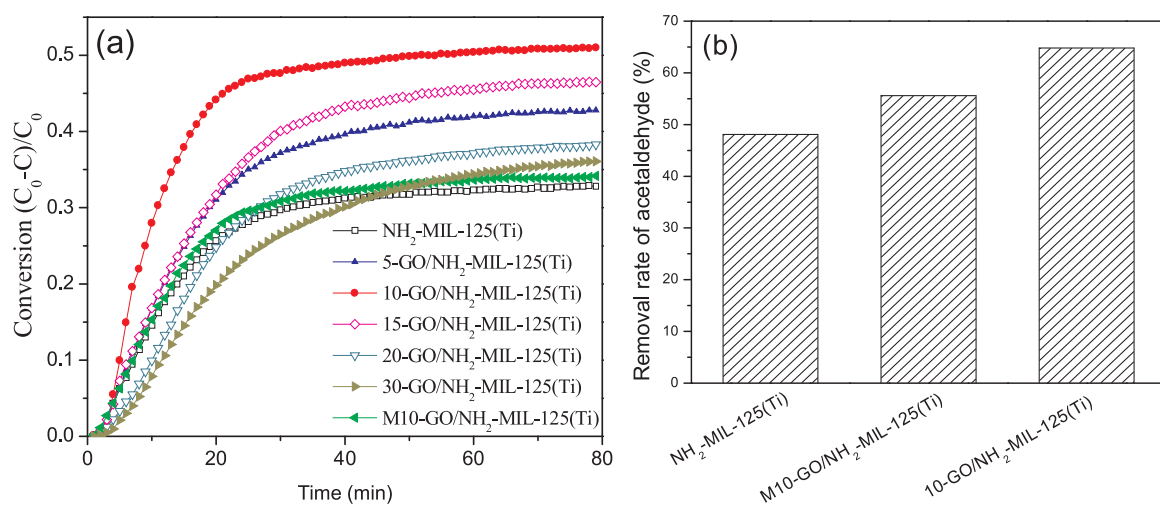
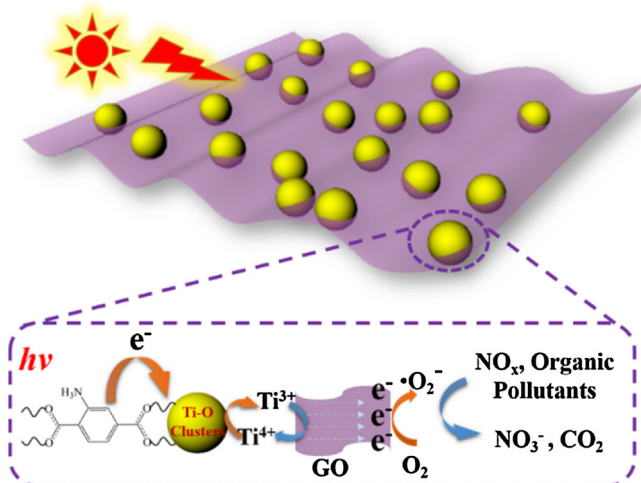


Fig. 8. (a) The photo-oxidation of NO under visible-light ($\lambda > 420$ nm, 300 W tungsten lamp) irradiation; (b) the photo-degradation of gaseous acetaldehyde under visible-light irradiation ($\lambda > 420$ nm, 300 W xenon lamp) in the presence of 50.0 mg catalyst, the initial $[\text{CH}_3\text{CHO}] = 1.95$ mg/L.



Scheme 1. The mechanism of GO/NH₂-MIL-125(Ti) for treating pollutants under visible light irradiation.

GO and NH₂-MIL-125(Ti), owing to the microwave solvothermal treatment, is the key to enhancing the activity for the strong capability to transfer the photo-generated electrons. Thus, it is reasonable that such excellent activity of the as-formed GO/NH₂-MIL-125(Ti) may be ascribed to the enhanced photo-generated electron transfer rate, low electron-hole recombination rate, and large surface area. For exploring the application in environmental remediation, the as-prepared samples were also utilized to treat gaseous acetaldehyde pollutants. As shown in Fig. 8b, the sample of 10-GO/NH₂-MIL-125(Ti) shows a high activity for oxidizing gaseous acetaldehyde under visible light irradiation with about 65% removal rate. Such value is much higher than that (48%) of the pure NH₂-MIL-125(Ti). Similar to the results of the photocatalytic oxidation of NO, the mechanical mixing sample (M10-GO/NH₂-MIL-125(Ti)) still exhibited a lower photocatalytic performance for oxidizing acetaldehyde owing to the weak interaction between GO and NH₂-MIL-125(Ti), with the comparison to the sample prepared via microwave solvothermal process. For better understanding a possible working mechanism of GO/NH₂-MIL-125(Ti) for treating gaseous pollutants was proposed in Scheme 1. Upon being irradiated with visible light, the ligand linker (H₂ATA) in the MOF crystals was excited for generating electrons [50]. The photogenerated electrons could transfer from the HOMO orbital to the LUMO orbital of the MOF [51], and they were further transferred to the center of the Ti–O clusters for reducing Ti⁴⁺ to Ti³⁺ [40]. Owing to the strong heterojunctions between GO and NH₂-MIL-125(Ti), such trapped electrons in the clusters can be fast accumulated on the surface of GO nanosheets, allowing more electrons to react with the O₂ molecules for producing oxygen radicals (·O₂⁻). Thus, both the NO_x and acetaldehyde could be further oxidized by these oxygen radicals for their strong oxidizing ability. Furthermore, the NO_x and acetaldehyde could be directly oxidized by the photogenerated holes on the HOMO orbital owing to its oxidizing ability. And the photogenerated holes could also react with the H₂O molecules to produce the hydroxyl radicals (·OH), which owned the strong oxidizing ability as well as the ·O₂⁻ [52]. Then NO_x and acetaldehyde could also be oxidized by the ·OH [53–55].

4. Conclusion

Highly crystallized NH₂-MIL-125(Ti) were *in-situ* dispersedly grafted on the surface of GO under the help of the hot-spot effect of GO under the microwave irradiation. Strong interaction between GO and NH₂-MIL-125(Ti) was obtained for the formation of heterojunctions. Both the high crystallinity and strong heterojunctions are highly favorable for enhancing photocurrent, electron carrier density and electron-

transfer rate from NH₂-MIL-125(Ti) to GO, and for inhibiting the electron-hole recombination to achieve high quantum efficiency. Under visible-light ($\lambda > 420$ nm) irradiation, the electrons generated from NH₂-MIL-125(Ti) could be fast transferred to GO through the heterojunctions. The trapped electrons on GO could further react with O₂ for the formation of oxygen radicals, allowing the oxidation of NO_x and acetaldehyde. The present work also supplied a microwave-induced platform for the fabrication of carbon materials enhanced MOF photocatalysts with highly efficient optical and electronic property.

Acknowledgements

This work was supported by National Natural Science Foundation of China (21477079, 21677099), the Ministry of Education of China (PCSIRT IRT 16R49), and the Shanghai Government (15QA1403300).

References

- [1] J.R. Li, R.J. Kuppler, H.C. Zhou, Chem. Soc. Rev. 38 (2009) 1477–1504.
- [2] H. Guo, F. Lin, J. Chen, F. Li, W. Weng, Appl. Organomet. Chem. 29 (2015) 12–19.
- [3] J. Lee, O.K. Farha, J. Roberts, K.A. Scheidt, S.T. Nguyen, J.T. Hupp, Chem. Soc. Rev. 38 (2009) 1450–1459.
- [4] H.L. Jiang, H. Liu, C. Xu, D. Li, Angew. Chem. Int. Ed. (57) (2018) 1–6.
- [5] L.J. Murray, M. Dinca, J.R. Long, Chem. Soc. Rev. 38 (2009) 1294–1314.
- [6] K. Sumida, D.L. Rogow, J.A. Mason, T.M. McDonald, E.D. Bloch, Z.R. Herm, T. Bae, J.R. Long, Chem. Rev. 112 (2012) 724–781.
- [7] X.C. Ma, L.Q. Li, R.F. Chen, C.H. Wang, H.L. Li, S.B. Wang, Appl. Surf. Sci. 435 (2018) 494–502.
- [8] J.R. Li, J. Sculley, H.-C. Zhou, Chem. Rev. 112 (2012) 869–932.
- [9] D.-X. Xue, Y. Belmabkhout, O. Shekhan, H. Jiang, K. Adil, A.J. Cairns, M. Eddaoudi, J. Am. Chem. Soc. 137 (2015) 5034–5040.
- [10] Z.G. Gu, W.Q. Fu, X. Wu, J. Zhang, Chem. Commun. 52 (2016) 772–775.
- [11] L.E. Kreno, K. Leong, O.K. Farha, M. Allendorf, R.P. Van Duyne, J.T. Hupp, Chem. Rev. 112 (2012) 1105–1125.
- [12] Y.H. Han, C.B. Tian, Q.H. Li, S.W. Du, J. Mater. Chem. C 2 (2014) 8065–8070.
- [13] M. Dan-Hardi, C. Serre, T. Frot, L. Rozes, G. Maurin, C. Sanchez, G. Férey, J. Am. Chem. Soc. 131 (2009) 10857–10859.
- [14] M.A. Nasalevich, R. Becker, E.V. Ramos-Fernandez, S. Castellanos, S.L. Veber, M.V. Fedin, F. Kapteijn, J.N.H. Reek, J.I. van der Vlugt, J. Gascon, Energy Environ. Sci. 8 (2015) 364–375.
- [15] K. Meyer, S. Bashir, J. Llorca, H. Idriss, M. Ranocchiari, A. van Bokhoven Jeroen, Chem. Eur. J. 22 (2016) 13894–13899.
- [16] F. Ye, H. Li, H. Yu, S. Chen, X. Quan, Appl. Surf. Sci. 426 (2017) 177–184.
- [17] H. Liu, J. Zhang, D. Ao, Appl. Catal. B: Environ. 221 (2018) 433–442.
- [18] Z. Wu, X. Huang, H. Zheng, P. Wang, G. Hai, W. Dong, G. Wang, Appl. Catal. B: Environ. 224 (2018) 479–487.
- [19] Y. Fu, L. Sun, H. Yang, L. Xu, F. Zhang, W. Zhu, Appl. Catal. B: Environ. 187 (2016) 212–217.
- [20] N.D. McNamara, G.T. Neumann, E.T. Masko, J.A. Urban, J.C. Hicks, J. Catal. 305 (2013) 217–226.
- [21] D. Jin, Q. Xu, L. Yu, X. Hu, Microchim. Acta 182 (2015) 1885–1892.
- [22] J. Liu, H. Bai, Y. Wang, Z. Liu, X. Zhang, D. Sun Darren, Adv. Funct. Mater. 20 (2010) 4175–4181.
- [23] N. Zhang, Y. Zhang, X. Pan, M.-Q. Yang, Y.J. Xu, J. Phys. Chem. C 116 (2012) 18023–18031.
- [24] J. Yu, M. Jaroniec, Appl. Surf. Sci. 430 (2018) 1.
- [25] X. Zeng, Z. Wang, G. Wang, T.R. Gengenbach, D.T. McCarthy, A. Deletic, J. Yu, X. Zhang, Appl. Catal. B: Environ. 218 (2017) 163–173.
- [26] C. Wang, X. Han, P. Xu, X. Zhang, Y. Du, S. Hu, J. Wang, X. Wang, Appl. Phys. Lett. 98 (2011) 072906.
- [27] K.S. Kumar, S. Pittala, S. Sanyadanam, P. Paik, RSC Adv. 5 (2015) 14768–14779.
- [28] D. Zhang, G. Li, X. Yang, J.C. Yu, Chem. Commun. (2009) 4381–4383.
- [29] M.C. Wen, P.J. Liu, S.-N. Xiao, K. Mori, Y. Kuwahara, H. Yasutaka, H. Yamashita, H.X. Li, D.Q. Zhang, RSC Adv. 5 (2015) 11029–11035.
- [30] D.C. Marcano, D.V. Kosynkin, J.M. Berlin, A. Sinitskii, Z.-Z. Sun, A. Slesarev, L.B. Alemany, W. Lu, J.M. Tour, ACS Nano 4 (2010) 4806–4814.
- [31] G.S. Li, B. Jiang, S.N. Xiao, Z.C. Lian, D.Q. Zhang, J.C. Yu, H.X. Li, Environ. Sci. Proc. Impact. 16 (2014) 1975–1980.
- [32] G.S. Li, D.Q. Zhang, J.C. Yu, M.K.H. Leung, Environ. Sci. Technol. 44 (2010) 4276–4281.
- [33] Y.H. Fu, D.R. Song, Y.J. Chen, R.K. Huang, Z.X. Ding, X.Z. Fu, Z.H. Li, Angew. Chem. Int. Ed. 51 (2012) 3364–3367.
- [34] G. Leofanti, M. Padovan, G. Tozzola, B. Venturelli, Catal. Today 41 (1998) 207–219.
- [35] G.S. Li, D.Q. Zhang, J.C. Yu, Chem. Mater. 20 (2008) 3983–3992.
- [36] S.J. Park, K.-S. Lee, G. Bozoklu, W.W. Cai, S.B.T. Nguyen, R.S. Ruoff, ACS Nano 2 (2008) 572–578.
- [37] W. Zhu, P.J. Liu, S.N. Xiao, W.C. Weng, D.Q. Zhang, Appl. Catal. B: Environ. 172 (2015) 46–51.
- [38] M. Nara, H. Torii, M. Tasumi, J. Phys. Chem. 100 (1996) 19812–19817.
- [39] M.S. Dresselhaus, A. Jorio, M. Hofmann, G. Dresselhaus, R. Saito, Nano Lett. 10

(2010) 751–758.

[40] J. Xu, S. He, H.L. Zhang, J.C. Huang, H.X. Lin, X.X. Wang, J.L. Long, *J. Mater. Chem. A* 3 (2015) 24261–24271.

[41] D.R. Sun, L. Ye, Z.H. Li, *App. Catal. B: Environ.* 164 (2015) 428–432.

[42] J.G. Yu, J. Jin, B. Cheng, M. Jaroniec, *J. Mater. Chem. A* 2 (2014) 3407–3416.

[43] L. Jia, D.H. Wang, Y.X. Huang, A.W. Xu, H.Q. Yu, *J. Phys. Chem. C* 115 (2011) 11466–11473.

[44] Y.W. Zhu, S. Murali, W.W. Cai, X.S. Li, J.W. Suk, J.R. Potts, R.S. Ruoff, *Adv. Mater.* 22 (2010) 3906–3924.

[45] G.S. Li, L. Wu, F. Li, P.P. Xu, D.Q. Zhang, H.X. Li, *Nanoscale* 5 (2013) 2118–2125.

[46] H.X. Li, G.S. Li, J. Zhu, Y. Wan, *J. Mol. Catal. Chem.* 226 (2005) 93–100.

[47] L.Q. Jing, Y.C. Qu, B.Q. Wang, S.D. Li, B.J. Jiang, L.B. Yang, W. Fu, H.G. Fu, J.Z. Sun, *Sol. Energy Mater. Sol. Cells* 90 (2006) 1773–1787.

[48] G.S. Li, Z.C. Lian, W.C. Wang, D.Q. Zhang, H.X. Li, *Nano Energy* 19 (2016) 446–454.

[49] Z.C. Lian, W.C. Wang, G.S. Li, F.H. Tian, K.S. Schanze, H.X. Li, *ACS Appl. Mater. Interfaces* 9 (2017) 16959–16966.

[50] X.J. Wang, X. Zhao, D.Q. Zhang, G.S. Li, H.X. Li, *Appl. Catal. B: Environ.* 228 (2018) 47–53.

[51] M.C. Wen, K. Mori, Y. Kuwahara, H. Yamashita, *ACS Energy Lett.* 2 (2017) 1–7.

[52] S.L. Wang, S.H. Lin, D.Q. Zhang, G.S. Li, M.K.H. Leung, *Appl. Catal. B-Environ.* 215 (2017) 85–92.

[53] Y. Ye, Z.G. Zang, T.W. Zhou, F. Dong, S.R. Lu, X.S. Tang, W. Wei, Y.B. Zhang, *J. Catal.* 357 (2018) 100–107.

[54] M.J. Chen, J. Yao, Y. Huang, H. Gong, W. Chu, *Chem. Eng. J.* 334 (2018) 453–461.

[55] X.L. Chen, H.Q. Zhang, D.Q. Zhang, Y.C. Miao, G.S. Li, *Appl. Surf. Sci.* 435 (2018) 468–475.